Observations of internal tides in the Mozambique Channel

A. M. M. Manders,[1] L. R. M. Maas, and T. Gerkema
Royal Netherlands Institute for Sea Research, Texel, Netherlands

Received 31 October 2003; revised 12 August 2004; accepted 8 November 2004; published 29 December 2004.

[1] Internal waves in the Mozambique Channel were studied, in the narrowest passage between Mozambique and Madagascar. Seven current meter moorings were deployed for a year and a half. The observed baroclinic flow in the semidiurnal frequency band exhibited strong intermittency. Internal tides could be detected at nearly all times from differences between current meter records in amplitude and phase, varying in time. To study the long-term average of the internal tidal field, the overall energy in the semidiurnal bands was computed for each location. Internal tidal currents were everywhere strongest near the surface (around 4 cm/s at 250 m depth up to 12 cm/s near the pycnocline in the generation area), decreased to less than 3 cm/s at 600 m depth, and increased a little near the bottom. The results were compared with numerical results from a two-dimensional internal-tide generation model allowing a description of beam scattering at the pycnocline and repeated reflection. Model results and observations were in qualitative agreement. *INDEX TERMS:* 4544 Oceanography: Physical: Internal and inertial waves; 4223 Oceanography: General: Descriptive and regional oceanography; 4255 Oceanography: General: Numerical modeling; *KEYWORDS:* internal waves, Mozambique Channel

Citation: Manders, A. M. M., L. R. M. Maas, and T. Gerkema (2004), Observations of internal tides in the Mozambique Channel, *J. Geophys. Res.*, *109*, C12034, doi:10.1029/2003JC002187.

1. Introduction

[2] This study presents the first observations of semidiurnal internal tides in the Mozambique Channel. Internal tides can be found nearly everywhere in the ocean. Near the shelf break, where they are generated by the barotropic tide, they may manifest themselves as beams [*Pingree and New*, 1991]. Some regions have been intensively investigated, like the Bay of Biscay [e.g., *Pingree and New*, 1991; *Lam et al.*, 2004], where internal wave beams are observed that propagate away from the generation area. Far away from the generation area, results are generally interpreted in terms of low vertical wave number modes.

[3] The angle α of energy propagation of the internal wave beam with respect to the vertical depends on the frequency ω, the Brunt-Väisälä-frequency N, and the Coriolis parameter f [*LeBlond and Mysak*, 1978],

$$\tan^2 \alpha = \frac{N^2 - \omega^2}{\omega^2 - f^2}. \quad (1)$$

This constraint on the direction of propagation yields the properties typical of internal waves, especially regarding reflection at slopes. Theoretically, in channel-shaped basins, wave attractors can be formed via geometric focusing due to repeated reflection [*Maas and Lam*, 1995]. This effect has indeed been observed in the laboratory [*Maas et al.*, 1997], but not yet in the ocean. We will discuss this aspect in relation to the data from the Mozambique Channel in the last section.

[4] In the present study, the distribution of semidiurnal internal waves in the Mozambique Channel is investigated, using data from an array of current meter moorings. The results are compared with a two-dimensional numerical internal-tide generation model for the research area.

2. Description of the Mozambique Channel

[5] The Mozambique Channel is a deep sea strait between the African continent and Madagascar. Figure 1a displays the research area. The detailed bathymetry of the cross section is shown in Figure 2. The steep topography and the reasonably strong surface tide of about 1 m for M_2 and S_2 [*LeProvost*, 2001] make the area in principle favorable for the generation of internal tides. The large-scale flows in the Mozambique Channel are strong but highly variable, especially in the narrowest part. Although their observations consisted of snapshots, *Schuman* [1998] and *DiMarco et al.* [2002] suggested that eddies might be responsible for this. This was confirmed in the long-term current meter study by *Ridderinkhof and De Ruijter* [2003], who showed that large anticyclonic eddies are formed in or slightly to the north of the observation area and subsequently pass southward through the channel. They extend over the full water column and have current velocities of 40 cm/s or more in

[1]Now at Royal Dutch Meteorological Institute (KNMI), De Bilt, Netherlands.

Copyright 2004 by the American Geophysical Union.
0148-0227/04/2003JC002187

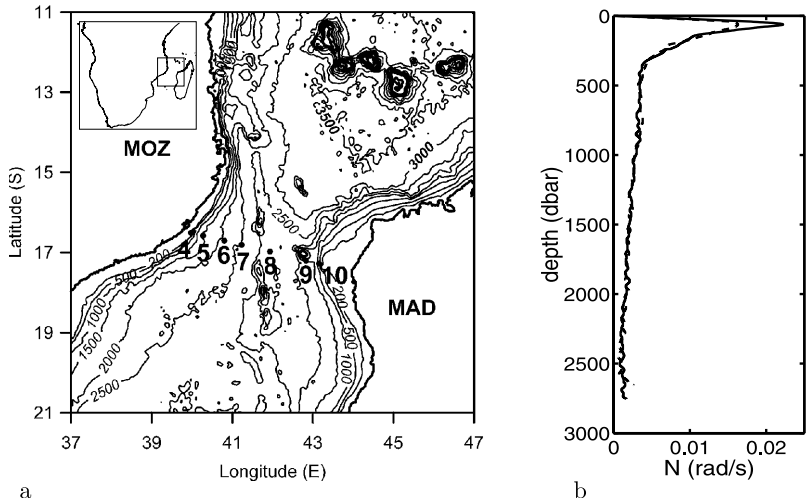

Figure 1. (a) Map of the research area with inset of a map of Southern Africa for orientation. Mozambique (MOZ) is on the left, and Madagascar (MAD) is on the right side. The mooring positions are indicated by the black dots (4–10). (b) The horizontally averaged Brunt-Väisälä-frequency (see text) for both cruises. The values for the 2000 cruise (dashed line) are nearly identical to those of 2001 (solid line), except for the pycnocline peak, which is less strong (0.016 rad/s in 2000 and 0.022 rad/s in 2001).

the upper few hundred meters. Four to five of such eddies are formed per year.

[6] Our data stem from the same mooring array as the data used by *Ridderinkhof and De Ruijter* [2003], but now the internal wave band is studied. The moorings were part of the Agulhas Current Source EXperiment (ACSEX). Two cruises with CTD-observations were undertaken with the Dutch RV *Pelagia*, in March–April 2000 and 2001. During these cruises the current meter moorings were (re)deployed (Figure 2) and finally recovered in November 2001, with the British RV *Charles Darwin*. According to lowered-ADCP observations [*Ridderinkhof and De Ruijter*, 2003] and CTD-profiles, the two cruises were in two different regimes: During the first cruise an eddy was present, bringing warmer water into the basin, as could be observed by the slight depression of the isotherms. During the second cruise, the pycnocline was much stronger. It had an arch-like structure with a shallow pycnocline in the middle, deepening toward the sides of the channel. An indication of the stratification is plotted in Figure 1b. Below the pycnocline, this is the cross-channel averaged value of $N(z)$. For the upper layer the cross-channel differences in pycnocline depth would lead to smearing of the pycnocline when $N(z)$ is averaged. To avoid this, representative values for the depth and strength of the peak were taken to construct an "average" profile. The average profiles of the first and the second cruise are identical except for the pycnocline strength: 0.016 rad/s and 0.022 rad/s, respectively.

[7] Both cruises were in March–April. We do not have observations in different seasons. Satellite observations reveal that the average surface temperature fluctuates from 25°C in July to the observed 29°C (www.emc.ncep.noa.gov/research/cmb/sst_analysis). The mixed layer depth is estimated from 70 m in July to 20 m in March–April [*Kara et al.*, 2002]. The two different observed stratifications are therefore not representative for a full year. But the observed difference in pycnocline strength is an important factor since it has consequences for the behavior of internal waves, as we will illustrate.

3. Observations

[8] We use the observations from the ACSEX program. As the mooring array was not specifically designed for internal wave detection, the separation is relatively large. This was further deteriorated by current meter damage and loss, especially during the first period. In the first period, the sampling frequency of the current meters was 3 cph (cycles per hour) and of the ADCPs was 1 cph. For the second period, these frequencies were doubled.

[9] The horizontal velocity measurements were decomposed into cross-channel (u) and along-channel (v) compo-

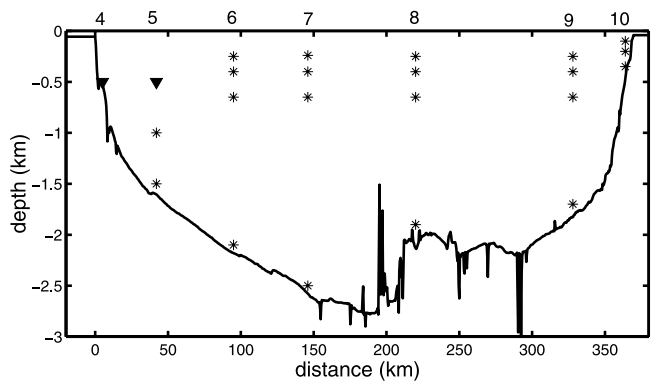

Figure 2. Bottom topography and distribution of current meters (stars) and upward-looking ADCPs (triangles) which cover the upper 500 m. Mozambique is on the left side and Madagascar is on the right. Numbers refer to the mooring identification numbers, and individual current meters were numbered from top (1) to bottom (4), irrespective of their recovery or functioning.

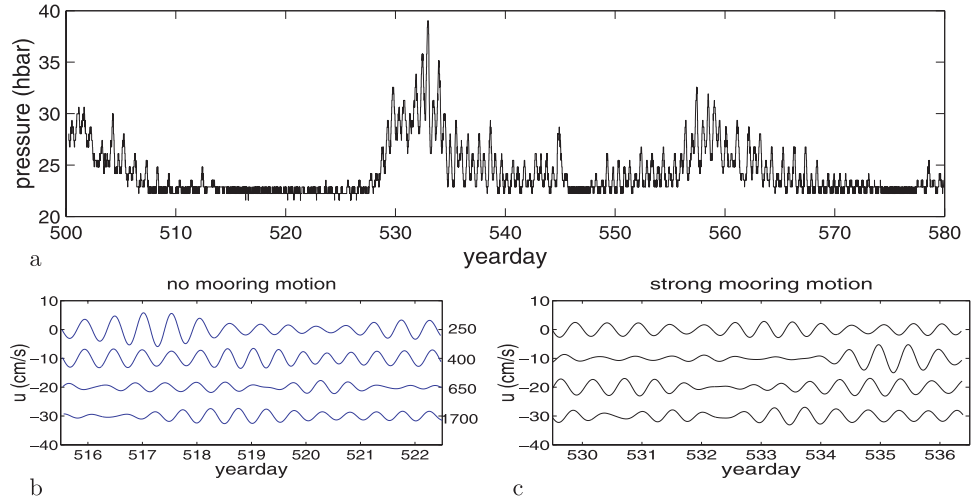

Figure 3. (a) Pressure signal of ACS09-1, showing strong pressure fluctuations indicating tilting of the mooring. Band-pass filtered (1.7–2.4 cpd) baroclinic signals of the four current meters of mooring ACS09, for a period with (b) nearly no mooring motion and (c) strong mooring motion.

nents; thus the geographical coordinate system is rotated clockwise about 14 degrees. Barotropic tidal currents were determined by taking vertical averages of the currents, which were high-pass filtered (cut-off frequency 0.25 cycles per day, cpd) to remove the dominant eddies, and fitting them to sine and cosine functions with tidal frequencies K_1, O_1, N_2, M_2, and S_2 (harmonic analysis [*Godin*, 1972]). The inertial frequency (0.58 cpd) was well away from the tidal frequencies. Barotropic tidal currents were mainly directed along-channel; harmonic analysis gave fairly consistent results of 2 to 5 cm/s for M_2 for v, depending on the local depth, and smaller contributions of the other tidal components. The five tidal components explained up to 80% of the currents. For u the velocity of tidal components was in general less than 1 cm/s, except close to the shelf, and the fit was generally well below 50%. The coherent barotropic tide was subtracted from the high-pass filtered signal to obtain the baroclinic currents, that were then of the same order for u and v.

[10] Owing to the strong currents, when a threshold value of the velocity was exceeded, the moorings were tilted and could move with the flow. The pressure signal (see Figure 3a for an example) and tiltmeter signals revealed that this tilt was up to 30°, and the threshold value was around 10 cm/s. If this threshold was exceeded, the mooring could move with the tidal currents. There was a rough proportionality between the observed tilt and the current velocity. Extremes were about 5° tilt fluctuations for tidal currents of about 12 cm/s (superimposed on a background tilt of 20° resulting from a background current of 40 cm/s). For a current meter at 1750 m from the bottom, this yields average velocities of the mooring of 0.6 cm/s. This is less than 10% of the observed tidal currents, and we assume that the velocity observations themselves are not corrupted substantially. Another aspect of the mooring motion is that a current meter covers a depth range instead of a fixed depth. This depth range is considerable for the longer moorings: The pressure sensors indicated that over eddy turnover time depth differences up to 200 m occurred. This aspect should be kept in mind when interpreting the data. We did not observe structural differences between periods when mooring motion was absent and periods when the mooring was tilted substantially (Figures 3b and 3c). During the second deployment period, two moorings drifted away a little (ACS06 about 20 km and ACS08 about 10 km; ACS refers to ACSEX, and the mooring identification numbers are given in Figure 2).

3.1. Intermittency

[11] In Figures 4 and 5 the band-pass filtered (1.7–2.4 cpd) baroclinic records u and v are directly shown for the two deployment periods for all available current meters. They illustrate the variations of amplitude with time. Near the shelf (mooring ACS10), motion was considerably stronger, which can be interpreted as the effect of the generation area where strong internal tides are expected. The signals appear to be highly irregular, and events of higher velocities of one current meter could not be related to similar events in other current meter records. There are beatings that resemble spring-neap cycles, but they are irregular. An enlargement, in which internal tides are clearly visible, is shown in Figure 6 for the four current meters of ACS09. The v-component was added for completeness. The change in amplitude cannot be purely attributed to a regular spring-neap cycle. The different current meter signals clearly have different phase and amplitude, especially for yeardays 595–600. Also, the phases and amplitudes of u and v of individual current meters vary incoherently. Differences between current meters may be related to the different position in the channel with respect to internal wave paths. However, the differences are not persistent, which may be caused by changes in background conditions (changes in wave paths) or changes in current meter position due to mooring motion, which could yield depression of the mooring up to 200 m. Intermittent behavior is generally encountered in long-time internal tide observations [*Magaard and McKee* ,1973; *Van Haren*, 2004; *Lerczak et al.*, 2003], with beatings with a period of about 5 days, as observed here.

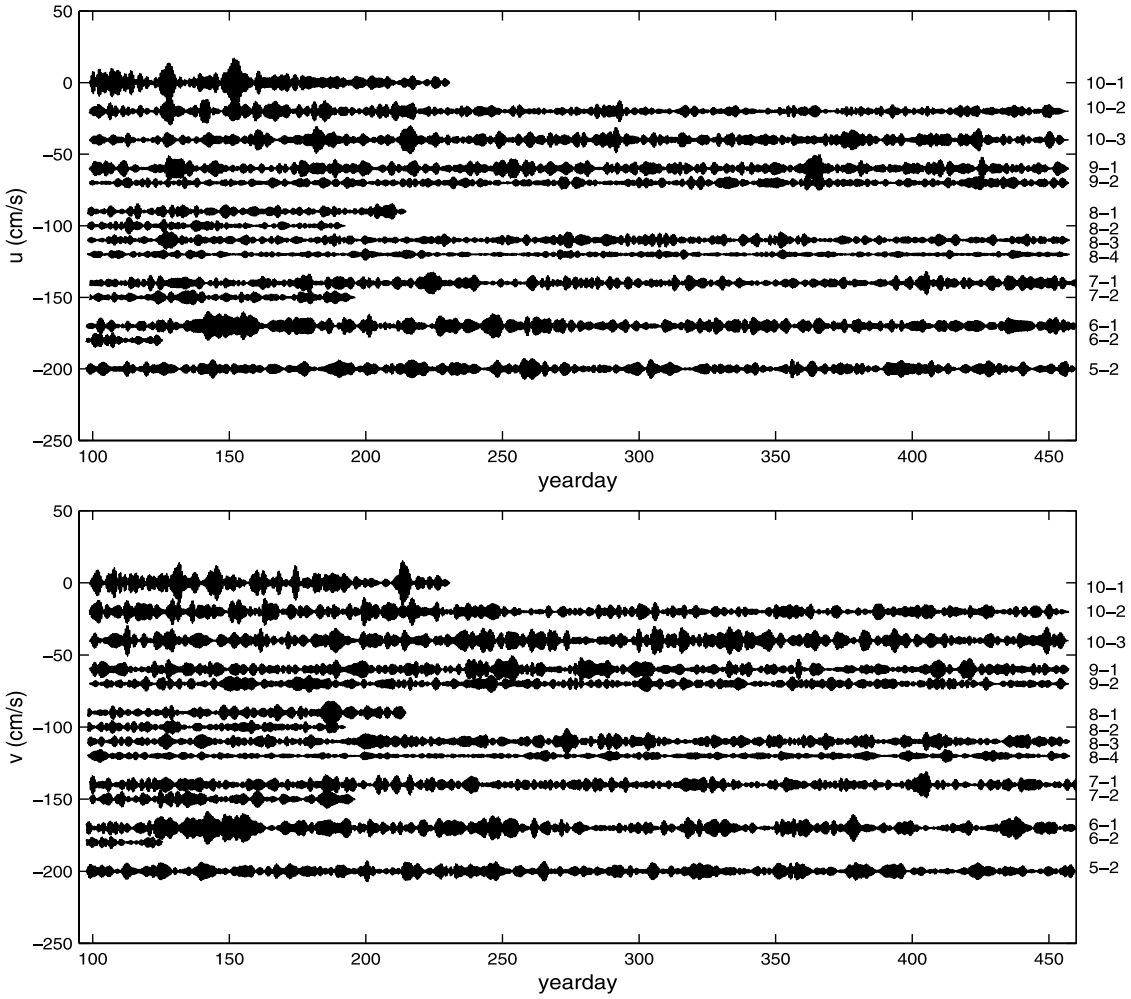

Figure 4. Band-pass filtered baroclinic records of u and v for the first year of observation. The scale is in cm/s, with vertical offsets for the different current meters. The numbers on the right indicate the mooring and current meter number (see also Figure 2). Yearday 0 refers to 1 January 2000, 0000 UTC.

[12] Owing to the strong intermittency, it is necessary to look at short periods when comparing different current meter observations. By harmonic analysis of the M_2-component only for windows of 4 days, we calculated amplitude and phase (changes) of the baroclinic band-pass filtered observations of the different current meters. Also cross-correlations were calculated for windows of 4 days for the baroclinic high-pass filtered observations. Both methods of analysis did not yield consistent results. Amplitudes and phases were varying slowly but continuously without a structural phase difference between the observations of different current meters. Only incidentally high cross-correlation values were found. This also follows from direct inspection of Figures 4 and 5. Regarding the wavelength of internal tides, the current meters were in general too far apart to expect high correlations and to use the array as an antenna to determine directions of propagation.

3.2. Spectra and Integrated Signal

[13] We were interested in the large-scale semidiurnal internal wave energy distribution in the channel. To quantify the average energy of the highly variable velocities, spectra were used. Energy from the tidal frequencies may have leaked to the sidebands as a result of the intermittency (incoherence) [*van Haren*, 2004]. Therefore the energy in the semidiurnal band (D_2, 1.8–2.1 cpd) and in small bands around M_2 (1.905–1.955 cpd) and S_2 (1.98–2.02 cpd) have been determined by integration of the spectra.

[14] The current meter records were corrected for the barotropic tide. The first and last day of recordings were discarded, since they were contaminated by the settling and recovery of the mooring. Welch's method was used with spectral intervals of 0.0176 cpd, which is enough to separate the tidal peaks of M_2 and S_2 and enables reasonable averaging (six windows or more). Results of the D_2-integrated results were consistent with calculations of the RMS velocity of the band-pass filtered baroclinic results (up to 20% difference). Results in the small M_2 and S_2 bands are less accurate due to the small number of bands over which integration occurs. This easily yields errors of about 0.2 cm^2 s^{-2}. Small values in these bands (compared to the D_2-integrated values) indicate a large spectral leakage. Despite the relatively large uncertainties, the D_2 results are accurate enough to discern differences

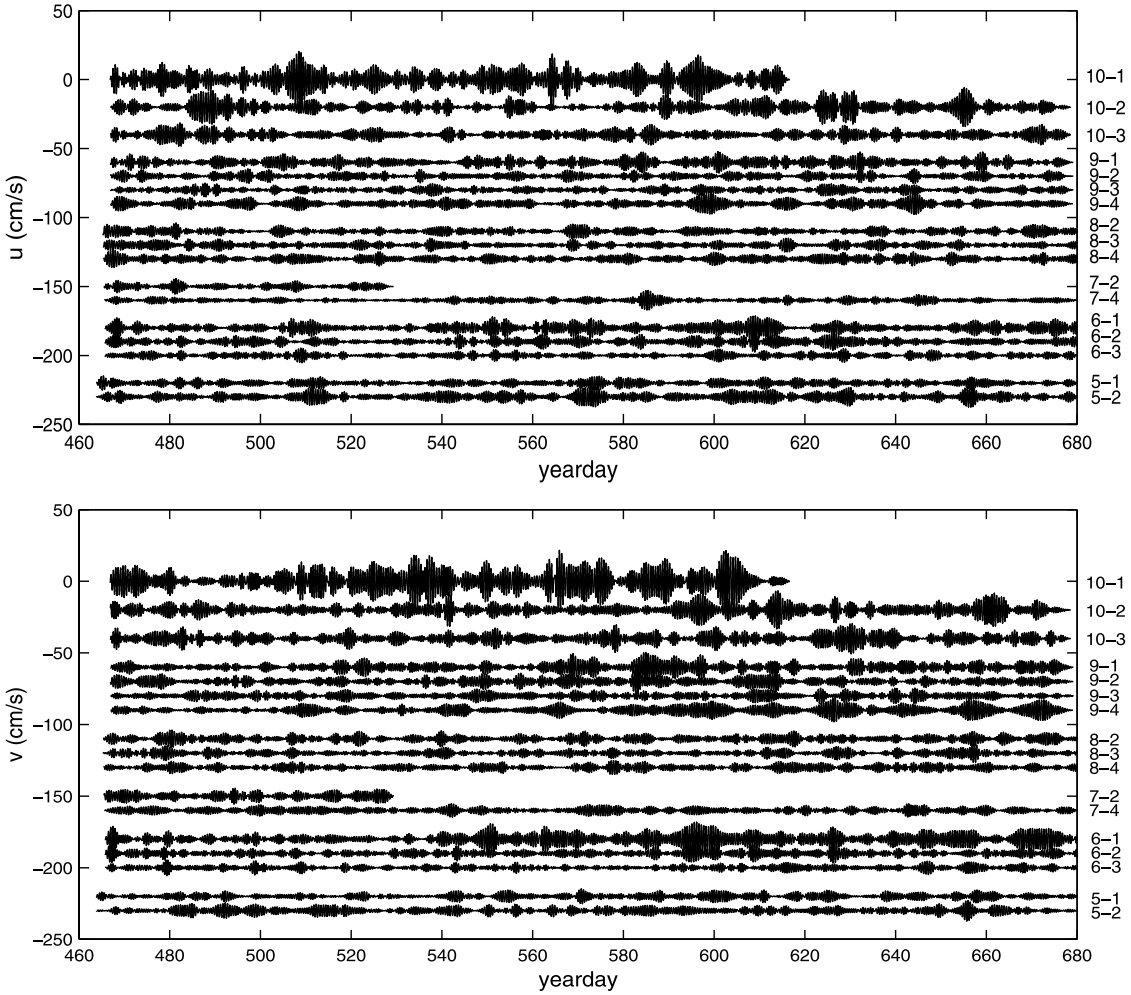

Figure 5. Same as Figure 4, for the second period of observation.

in amplitude. For the ADCP-records of ACS04-A and ACS05-A the spectra per bin were calculated. The results for the ADCP are shown in Figure 7 and provide insight in the vertical structure. All results are collected in Table 1. For current meters that did not function long enough (less than 2 months), just the band-pass filtered baroclinic RMS velocity is given without separation into an M_2 and an S_2 band.

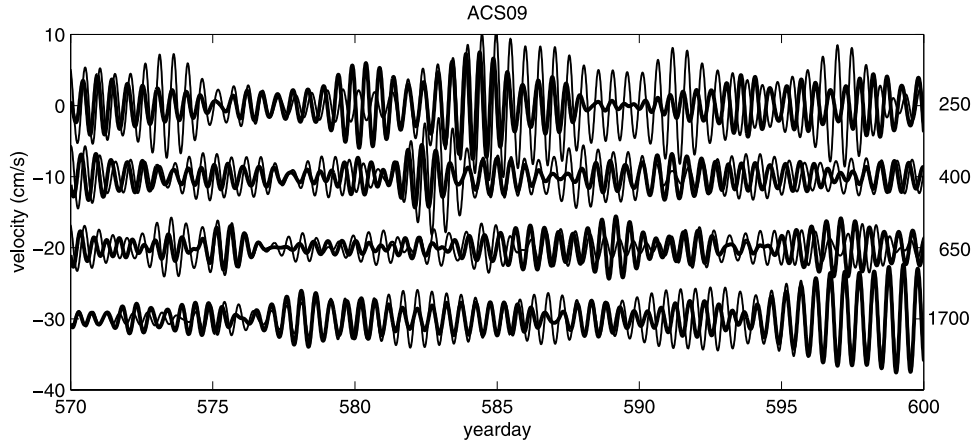

Figure 6. Amplitude and phase in the vertical of the four ACS09 current meters for u (thick line) and v (thin line). Yearday 0 refers to 1 January 2000, 0000 UTC. Internal waves are especially clear for yeardays 595–600, but phase differences can be found at nearly all times. The phases of u and v differ nearly continuously with respect to each other; sometimes the baroclinic tidal currents are rectilinear, sometimes they are nearly circular.

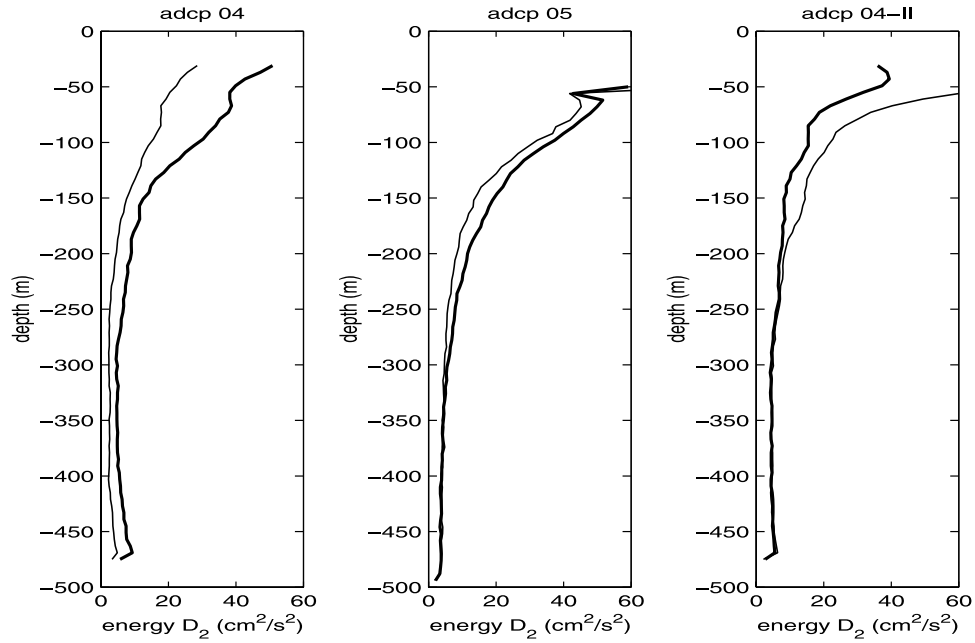

Figure 7. D_2 integrated spectra of the ADCPs for u (thick line) and v (thin line). The barotropic tide has been subtracted. The first two panels are for the first period of observation, and the third panel is for the second period.

[15] The results for the two mooring periods are roughly comparable. Notable exceptions are the upper current meters of ACS10. During the first period, the rotors of the mechanical current meters were heavily affected by biofouling and the observed velocities become too small over time. For the second period, acoustic current meters were used at these positions. The lower current meter of ACS08 also gives two different results. At this mooring position, the bottom has a strong and irregular topography. It may well be that during the first period the current meter was shielded by ridges. The mooring drifted about 10 km away during the second period, and the observations are thus mainly at a different site. The difference in strength of the v-component in ACS04 is remarkable. We could not find an explanation for this. For ACS09 the RMS velocity for the current meter at the bottom became larger after subtraction of the barotropic tide (from 2.97 to 3.92 $cm^2\ s^{-2}$) but also, before the subtraction, the RMS velocity in the semidiurnal tidal band was larger than for the middle current meters, albeit the difference was very small (10%). In general, the velocities were highest for the upper current meter, and near the bottom, velocities were slightly higher than in the middle of the water column.

[16] Internal tides are strongest near the shelf edge (upper observations of ACS10 and the ADCPs). This is in accordance with the common idea that the shelf edge is the generation area. The submaxima at a depth of 70–100 m of ACS04 (Figure 7) may be a manifestation of the downward propagating wave ray. The upper bins are in the pycnocline area. Toward the bottom, currents are a little intensified. Also, for the other moorings, motion is strongest for the upper current meter. However, the bottom currents are slightly stronger than the currents in the middle. The current meters are all well below the pycnocline.

3.3. Numerical Internal-Tide Generation Model

[17] The observations were compared with the results from a numerical internal-tide generation model. Under the assumption of along-slope uniformity, in this model [*Gerkema*, 2002] the observed topography and average stratification $N(z)$ (Figure 1b) were used to calculate the internal tidal currents generated by barotropic flow over topography. The barotropic cross-channel flux was prescribed, based on a velocity of 1 cm/s in the deep sea. A model run spanned 100 tidal periods, which appeared enough to overcome the transient response. The internal tidal current amplitudes of u were calculated for the stratification with and without eddy and are displayed in Figure 8. Two amplitude distributions are shown: one with absolute amplitudes and one where the velocity was scaled by $\sqrt{N(z)}$. This so-called WKB scaling [*Gill*, 1982] is used to separate adiabatic effects of the pycnocline on the velocities from concentration of energy due to repeated reflection and scattering, in which we are particularly interested.

[18] Motion is strongest near the surface for both stratification regimes. In general, motion is stronger for the stronger stratification around the pycnocline. Despite the fact that in the deep-sea the stratification is nearly identical, clearly the difference around the pycnocline has important consequences. For the stratification with eddy, energy is concentrated in the western part of the basin; this is less so for the situation without eddy. In both cases, there seems to be some beam scattering [*Gerkema*, 2001], as evidenced by the strong currents in the mixed layer (Figure 8b). The scaled velocities show the impor-

Table 1. Spectral Energy Integrated Over Tidal Bands (E) for u and v, in cm^2 s^{-2}[a]

Water Depth, m	Mooring	Design Depth, m	u			v		
			M2	S2	D2	M2	S2	D2
			First Period of Observation					
536	04A	50	11.21	6.57	38.22	6.28	4.04	20.46
	A	150	3.11	1.53	12.53	1.92	1.28	7.58
	A	250	1.35	1.01	6.56	0.58	0.37	2.66
	A	350	1.04	1.03	4.77	0.52	0.46	2.48
	A	450	2.06	1.30	7.46	0.87	0.82	3.80
1595	05A	50	22.51	6.62	51.56	15.24	7.92	44.77
	A	150	7.64	2.23	18.99	3.66	2.24	13.38
	A	250	2.73	0.96	7.98	1.63	0.96	5.74
	A	350	1.35	0.66	4.42	1.25	0.66	4.06
	A	450	1.01	0.65	3.75	1.18	0.83	4.16
		1498	1.88	0.63	4.36	2.11	0.74	5.17
2199	06	250	3.60	1.21	7.55	4.73	1.29	8.89
		400			2.76			2.19
2603	07	250	0.97	0.34	3.57	1.18	0.76	4.18
		400			2.94			3.49
1998	08	250			3.05			4.54
		400			1.98			2.64
		650	0.64	0.29	2.42	1.77	0.59	4.11
		1901	0.32	0.13	0.88	0.54	0.3	1.21
1815	09	360	1.89	0.78	5.22	2.29	1.03	5.51
		670	0.68	0.31	1.90	1.49	0.26	3.09
445	10	100			13.99			14.39
		200	1.23	0.56	4.13	2.60	0.74	5.54
		349	2.60	0.74	5.74	3.45	1.05	8.24
			Second Period of Observation					
536	04A	50	11.37	6.06	31.74	19.22	12.32	62.29
	A	150	1.41	1.86	8.20	2.80	3.39	14.51
	A	250	1.14	1.26	5.91	1.71	1.26	6.46
	A	350	0.71	1.01	4.72	1.39	0.75	4.74
	A	450	1.24	1.06	5.07	1.89	0.96	5.37
1595	05	1000	0.90	0.38	2.66	1.01	0.34	2.33
		1498	2.06	0.76	5.47	1.47	0.20	3.13
2199	06	250	3.10	1.04	6.02	6.89	1.88	11.27
		400	0.89	0.39	2.80	0.67	0.28	2.34
		650	0.49	0.15	1.60	0.29	0.2	1.48
2603	07	400			2.39			4.18
		2507	0.38	0.19	1.61	1.7	0.31	2.32
1998	08	400	0.50	0.55	2.26	0.83	0.35	2.59
		650	0.51	0.73	2.32	0.53	0.40	1.82
		1901	0.74	1.57	3.27	0.51	0.35	2.36
1815	09	250	1.93	0.55	5.04	2.98	0.60	6.30
		400	0.78	0.23	2.22	1.88	0.58	3.96
		650	0.56	0.30	1.81	0.91	0.69	3.24
		1719	1.70	2.00	4.83	2.75	1.23	5.03
445	10	100	11.29	4.83	27.73	19.56	5.24	38.07
		200	4.30	1.03	10.26	2.76	0.65	8.14
		349	1.82	0.60	4.96	2.76	0.87	7.99

[a]The A stands for ADCP. Where only a short period of observation is available due to current meter failure, the baroclinic band-passed RMS value is given.

tance of repeated bottom reflection, yielding patches of stronger internal wave motion. Phase patterns (Figure 8c) are in accordance with the patterns of strong motion. They show large-scale beams, crossing the channel in a few reflections, but these patterns are perturbed by interaction with other wave beams and beam scattering. It is difficult to separate these effects. They both result in small-scale variations.

[19] The observed integrated spectral energy in the semidiurnal band was translated into velocity amplitudes according to $2\sqrt{E_{D2}}$ and was also plotted in Figure 8 (in the small circles). The same observational results are plotted for both stratification regimes, since they are time-integrated results covering several eddy passages and the ''neutral'' in-between periods. The time-varying stratification also prohibits the use of a WKB scaling for these observed velocity amplitudes. The numerical results are in qualitative agreement with the observations. The large values observed in the upper ADCP observations and ACS10 were reproduced by the model. For the deeper current meters, the differences in the current strength are less prominent. It is not sensible to compare the phases of the integrated spectrum, as it was especially the variability of the phases that led us to use an integrated spectrum.

4. Discussion

[20] This paper presents the first study on semidiurnal internal tides in the Mozambique Channel. The current meter signals revealed highly variable internal tides, so that

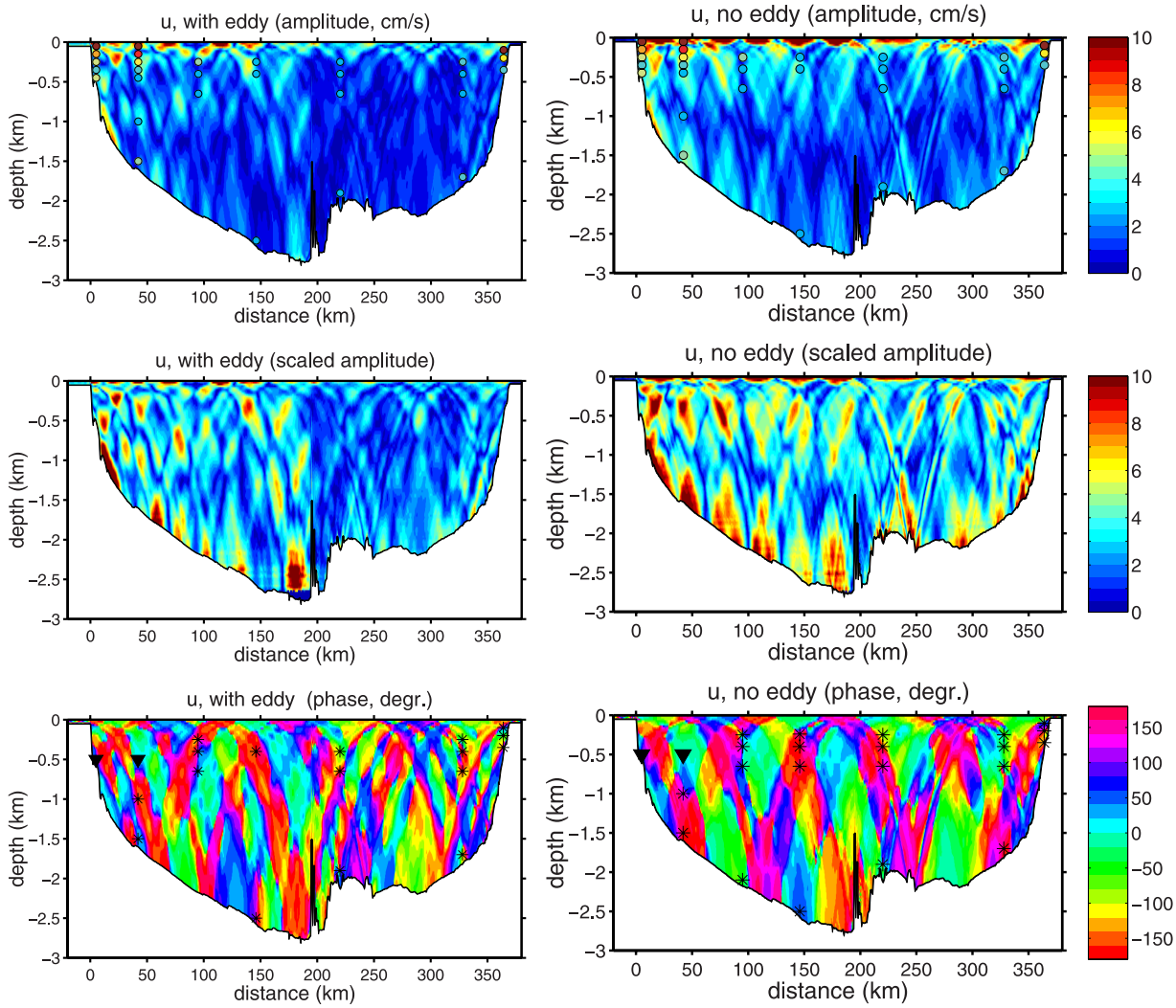

Figure 8. (top) Amplitude (cm/s), (middle) WKB-scaled amplitude, and (bottom) phase of the velocities from the numerical internal-tide generation model, for both stratification regimes (left-hand panels with eddy, right-hand panels without eddy). Solid circles are the observed amplitudes, calculated from the integrated spectra of the semidiurnal band. Stars and triangles indicate the position of the ADCPs and the current meters in the phase pictures.

it is not possible to speak of " the" internal wave field. This intermittency is possibly related to changes in wave ray paths due to the passage of eddies, which alters the stratification, and to changes in current meter positions due to strong currents; as was argued by *Gerkema* [2002], even a small disturbance of the ray path can result in an intermittent signal, especially if more than one tidal component is involved. The small scales of locations of strong motion and the phase patterns are in accordance with the strong intermittency, both due to changes in stratification and mooring motion. The observations resemble the classical case of intermittency in long-term observations on internal waves [*Magaard and McKee*, 1973], which were made in the western North Atlantic where eddies pass that are shed off by the Gulf stream, also resulting in a different stratification. However, we could not establish a direct connection between amplitude and phase changes of the internal waves and the passage of eddies. In the work of *van Haren*, [2004], the contributions of the different tidal frequencies M_2, S_2, and N_2 could be separated in time, and variations in their maxima could be interpreted as changes in ray path. Owing to the strong mooring motion, this is not possible here.

[21] The strongly intermittent character of the signal led us to consider the long-time averages of the semidiurnal baroclinic current amplitudes. It then appears that the strongest signals are predominantly located in the upper part of the water column. This is also what the model shows. The pattern becomes particularly complicated due to beam scattering at the pycnocline and the multiple reflections back into the basin. Multiple reflections in a basin of sloping walls can in principle lead to the formation of internal-wave attractors, as was shown by *Maas et al.* [1997]. In that study, a constant stratification was considered, so that internal scattering of beams is excluded. Using ray-tracing, simple M_2 or S_2 wave attractors could not be found for the Mozambique Channel for the observed stratification. Nonetheless, the numerical results suggest that for a certain stratification regime, the energy may become largely concentrated in the western half of the basin

(Figure 8). Apart from the fact that the existence of attractors depends on the exact topography and stratification (it may exist for other frequencies, but not for the tidal frequencies), beam scattering may oppose the focusing effect of the topography and prevent the appearance of attractors.

[22] We still think that it is important to consider repeated reflection in a channel like this. The basin is so narrow that an internal wave will probably reach the other side, since they are thought to survive about 10 reflections (and more for the lowest vertical mode), despite the scattering, and interfere with the direct wave rays. This might explain the weak submaximum of the ADCP near the Mozambiquan shelf where a stronger direct beam was expected. Also, the strong intermittency points to relatively small scales and a beam-like character of internal waves. Unfortunately, our current meters were too far apart to find more evidence for the validity of the numerical model. New observations in the deep sea and a better resolution of the upper part of the water column would be necessary for this.

[23] **Acknowledgments.** We thank H. Ridderinkhof for supervising the observational program and the crews of the *Pelagia*, *Charles Darwin*, and *Bazaruto* for their assistance. The detailed comments of two anonymous reviewers on an earlier version are greatly appreciated. A. M. was supported by the Dutch Organisation for Scientific Research NWO (project number 620-61-392).

References

DiMarco, S. F., P. Chapman, W. D. Nowlin Jr., P. Hacker, K. Donohue, M. Luther, G. C. Johnson, and J. Toole (2002), Volume transport and property distributions of the Mozambique Channel, *Deep Sea Res., Part II*, *49*, 1481–1511.

Gerkema, T. (2001), Internal and interfacial tides: Beam scattering and local generation of solitary waves, *J. Mar. Res.*, *59*, 227–255.

Gerkema, T. (2002), Application of an internal tide generation model to baroclinic spring-neap cycles, *J. Geophys. Res.*, *107*(C9), 3124, doi:10.1029/2001JC001177.

Gill, A. E. (1982), *Atmosphere-Ocean Dynamics*, Academic, San Diego, Calif.

Godin, G. (1972), *The Analysis of Tides*, Univ. of Toronto Press, Toronto, Ont., Canada.

Kara, A. B., P. A. Rochford, and H. E. Hurlburt (2002), Mixed layer depth (NMLD) climatologies, *Rep. NRL/FR/7330-02-9995*, Naval Res. Lab., Washington, D. C.

Lam, F.-P. A., L. R. M. Maas, and T. Gerkema (2004), Spatial structure of tidal and residual currents as observed over the shelf break in the Bay of Biscay, *Deep Sea Res., Part II*, *51*, 1075–1096.

LeBlond, P. H., and L. A. Mysak (1978), *Waves in the Ocean*, 602 pp., Elsevier, New York.

LeProvost, C. (2001), Ocean tides, in *Satellite Altimetry and Earth Sciences*, edited by L.-L. Fu and A. Cazenave, Academic, San Diego, Calif.

Lerczak, J. A., C. D. Winant, and M. C. Hendershott (2003), Observations of the semidiurnal internal tide on the southern California slope and shelf, *J. Geophys. Res.*, *108*(C3), 3068, doi:10.1029/2001JC001128.

Maas, L. R. M., and F.-P. A. Lam (1995), Geometric focusing of internal waves, *J. Fluid Mech.*, *300*, 1–41.

Maas, L. R. M., D. Benielli, J. Sommeria, and F.-P. A. Lam (1997), Observation of an internal wave attractor in a confined, stably statified fluid, *Nature*, *388*, 557–561.

Magaard, L., and W. D. McKee (1973), Semidiurnal tidal currents at 'site D,' *Deep Sea Res*, *20*, 997–1009.

Pingree, R. D., and A. L. New (1991), Abyssal penetration and bottom reflection of internal tide energy in the Bay of Biscay, *J. Phys. Oceanogr.*, *21*(1), 28–39.

Ridderinkhof, H., and W. P. M. de Ruijter (2003), Moored current observations in the Mozambique Channel, *Deep Sea Res., Part II*, *50*, 1933–1955.

Schuman, E. H. (1998), The coastal ocean off southeast Africa, including Madagascar, in *The Sea*, vol. 11, chap. 19, pp. 557–581, John Wiley, Hoboken, N. J.

van Haren, H. (2004), Incoherent internal tidal currents in the deep-ocean, *Ocean Dyn.*, *54*, doi:10.1007/s10236-003-0083-2.

T. Gerkema and L. R. M. Maas, Royal Netherlands Institute for Sea Research, PO Box 59, 1790 AB Den Burg, Netherlands. (gerkema@nioz.nl; maas@nioz.nl)

A. M. M. Manders, Royal Dutch Meteorological Institute (KNMI), P.O. Box 201, NL-3730 AE De Bilt, Netherlands. (manders@knmi.nl)